



Die Grenzen der
Chemie neu ausloten?
It takes
#HumanChemistry

Wir suchen kreative Chemikerinnen und Chemiker,
die mit uns gemeinsam neue Wege gehen wollen –
mit Fachwissen, Unternehmertum und Kreativität für
innovative Lösungen. Informieren Sie sich unter:

[evonik.de/karriere](https://www.evonik.de/karriere)

Self-Organization Postprocess for Additive Manufacturing in Producing Advanced Functional Structure and Material

Jinchun Chi,* Boris Agea Blanco, Giovanni Bruno, Jens Günster, and Andrea Zocca

Additive manufacturing (AM) is developing rapidly due to its flexibility in producing complex geometries and tailored material compositions. However, AM processes are characterized by intrinsic limitations concerning their resolution and surface finish, which are related to the layer-by-layer stacking process. Herein, a self-organization process is promoted as an approach to improve surface quality and achieve optimization of 3D minimal surface lightweight structures. The self-organization is activated after the powder bed 3D printing process via local melting, thereby allowing surface tension-driven viscous flow. The surface roughness R_a (arithmetic average of the roughness profile) could be decreased by a factor of 1000 and transparent lenses and complex gyroid structures could be produced for demonstration. The concept of self-organization is further elaborated by incorporating external magnetic fields to intentionally manipulate magnetic particles, which are mixed with the polymer before printing and self-organization. This concept can be applied to develop programmable materials with specific microtextures responding to the external physical conditions.

the part surface to the printing plane. Depending on the specific AM technology, other factors can contribute to the overall surface quality of the printed components. A well-known example is powder bed fusion, in which partially molten particles stick to the surface of the part, thus increasing the overall surface roughness.^[1]

The optimization of processing and material parameters to improve the surface quality and the microstructural homogeneity is a key research area in the field of AM.^[2] Decreasing the layer thickness has a fundamental impact on the surface quality and its effect is vastly studied,^[3–7] but it comes at a cost of a longer building time and lower throughput. An approach to decrease the stair stepping effect without sacrificing the productivity, as described, for example, by Turner et al.,^[8] is to align the stacking orientation parallel or perpendicular to the critical surfaces. In addition, in situ monitoring and closed-loop control

can also be implemented to improve the bulk homogeneity by which the material discontinuities caused by process disparity are monitored and reduced.^[9]

Different postprocessing methods are also available to improve the surface quality of AM components, with a wide range of applicable technologies depending on the material and application used. Ali et al.^[10] report an 80% improvement of surface roughness by electrochemical methods for the laser powder bed fusion process. Kumbhar et al.^[11] review the application of vibratory grinding, vibratory abrasion finishing, and ultrasonic abrasion finishing technologies as postprocesses for complex geometries. By these postprocessing strategies, the surface finishing can be improved to a range of several micrometers.

Specifically for polymeric components produced by fused deposition modeling (FDM), postprocessing in acetone vapor can be used to dissolve the microstairs on the surface of the part. Kuo et al.^[12] reported for acrylonitrile butadiene styrene (ABS) parts an improvement in surface roughness R_a by 98%, from several micrometers down to tens of nanometers.


Polymeric parts produced by AM from powder feedstocks are generally limited to having a rough surface and residual porosity (the latter especially for binder jetting). To address this issue, this article presents a self-organization process, which approaches the challenge of improving the surface quality and microstructural homogeneity of printed parts from powdery porous to fully dense. The self-organization is realized by locally melting the printed part in determined areas, which are defined during

1. Introduction

Since about three decades, additive manufacturing (AM) has been a field of active scientific research and is entering more into industrial production because it provides high flexibility in producing multiscale complex geometries. As intrinsic to the layer-by-layer forming process, in AM, a 3D object is sliced into 2D cross sections. This discrete principle brings inevitable limitations in terms of surface roughness and layer-to-layer bonding, inducing inhomogeneities in the surface and bulk of the material and in turn having an impact on the quality and mechanical strength of the printed part.

The stacking of layers with finite thickness causes the so-called “stair stepping effect,” which is dependent on the inclination of

J. Chi, B. Agea Blanco, G. Bruno, J. Günster, A. Zocca
Division 5.4 Advanced Multi-materials Processing
Bundesanstalt für Materialforschung und -prüfung (BAM)
12203 Berlin, Germany
E-mail: jinchun.chi@bam.de

 The ORCID identification number(s) for the author(s) of this article can be found under <https://doi.org/10.1002/adem.202101262>.

© 2021 The Authors. Advanced Engineering Materials published by Wiley-VCH GmbH. This is an open access article under the terms of the Creative Commons Attribution License, which permits use, distribution and reproduction in any medium, provided the original work is properly cited.

DOI: 10.1002/adem.202101262

printing. By the controlled viscous flow of the melted material, which is driven by surface tension, the interfaces between layers and between powder particles are eliminated, leading to a much denser material with a smooth surface

This approach differs profoundly from other kinds of postprocessing. First, here the AM and the postprocess are fully interconnected. The control of the shape evolution requires defining a certain volume of the part, which acts as a frame, and the remaining volume (defined as “filler”) that melts and self-organizes. In other terms, the frame material determines the boundary conditions for the self-organization of the molten material. In our approach, both the frame and the filler are defined already in the AM process, thus fully connecting the AM process and the postprocess. This is achieved using two print heads, the first of which is printing into the frame material a crosslinking additive and the second used for the filler material without crosslinker. This way, the information for self-organization is already inscribed during layer-by-layer binder jetting.

Furthermore, the reorganization of the surface structure follows surface energy gradients and is not predetermined, as it is in surface machining. This makes the self-organization in perspective attractive for fabricating components with a shape which can be predicted by simulations or by mathematical functions, such as structures inspired by lightweight minimal surfaces. Ragelle et al.^[13] proposed a similar surface tension-assisted method in additive manufactured-fenestrated scaffolds with a suspended liquid film. However, with this approach, self-organization is not well defined, as the amount of material offered is hardly controlled by immersing a solid body into a liquid phase. The volume engaged in self-organization is simply the result of an interplay of gravitational force and surface tension of the liquid phase on the solid preform. Thus, only the shape of membranes can be theoretically predicted. In this case, AM and postprocess are not fully interconnected, because only the frame is defined by AM.

The present process was introduced in a former publication, in which 2D parts with optical transparency were obtained.^[14] The self-organization in 3D structures is further developed in this article, which shows the potential capability for the self-organization of complex geometries.

In the second part of this article, a further elaboration of this concept is described, in which particle alignment under the driving force of a magnetic field was realized to tailor the microstructural texture. A considerable amount of research has been devoted to anisotropic texturing and tailoring material properties, such as piezoelectricity, optical, electronic, and mechanical properties.^[15–17] In this self-organization process, the transitional liquid phase allows the almost free motion of ferromagnetic particles, that can be aligned under the manipulation of an external magnetic field. In the future, this method can be used for local programming of material properties of 3D-printed parts.

2. Experimental Section

To demonstrate the self-organization of 3D complex geometries, the 3D model of a gyroid triply periodical minimal surface (TPMS) membrane structure was created, as shown in **Figure 1**. The gyroid is an infinitely connected TPMS structure

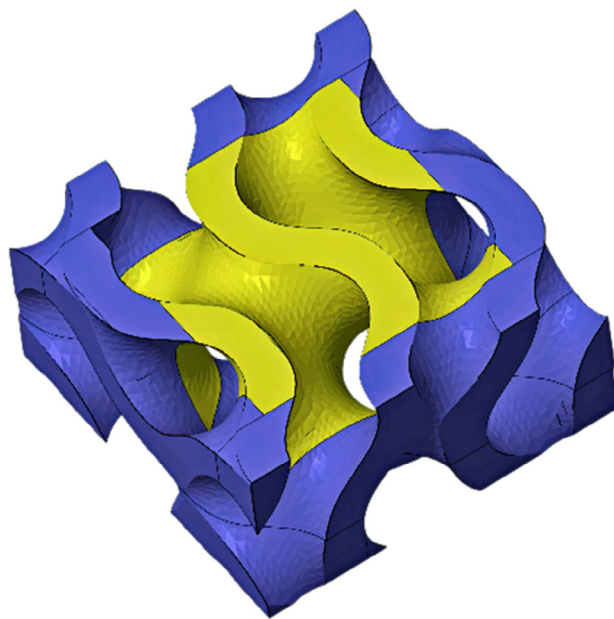


Figure 1. CAD design of gyroid TPMS membrane structure. The top and bottom surfaces of the frame (blue color) are cut out to show the internal filler structure (yellow color).

known to be lightweight and have high strength-to-weight ratio. The equation for a gyroid can be trigonometrically approximated as

$$\cos(x) \sin(y) + \cos(y) \sin(z) + \cos(z) \sin(x) = 0 \quad (1)$$

The gyroid TPMS lattice structure was generated by Mathematica (Wolfram Research, UK) with wall thickness of 3 mm and the total dimensions of 26 mm in X and Y directions (equal to one-unit cell) and 14 mm in Z direction. The gyroid model was then cut into two separate solids sliced by Netfabb software (Autodesk, USA). The outer area in blue color (**Figure 1**) was assigned as the rigid frame, thus defining the boundary conditions for self-organization. The inner part in yellow color was assigned as the filler, which can melt and flow enabling self-organization.

The composite model was produced by a two-color binder jet printing machine (Voxeljet Technology GmbH, Teststand VTS16, Germany). As illustrated in **Figure 2**, the yellow solid (filler) was assigned to printhead 1 and the blue solid (frame) was assigned to printhead 2. The second printhead printed binder containing a crosslinking agent, which crosslinked the powder into a thermoset matrix serving as the stable boundary (frame) during the self-organization postprocess.

The polymeric powder was a polymethylsilsesquioxane powder (Silres MK polymer, Wacker Chemie, Burghausen, Germany), designated as MK. The pure MK polymer had a softening temperature of 45–60 °C, but it can be crosslinked by catalyzed polycondensation of hydroxyl and ethoxyl groups. The unmodified MK polymer was soluble in different common solvents, which allowed using a solvent as binder in the binder jetting process. The printed binder thus partially dissolved the

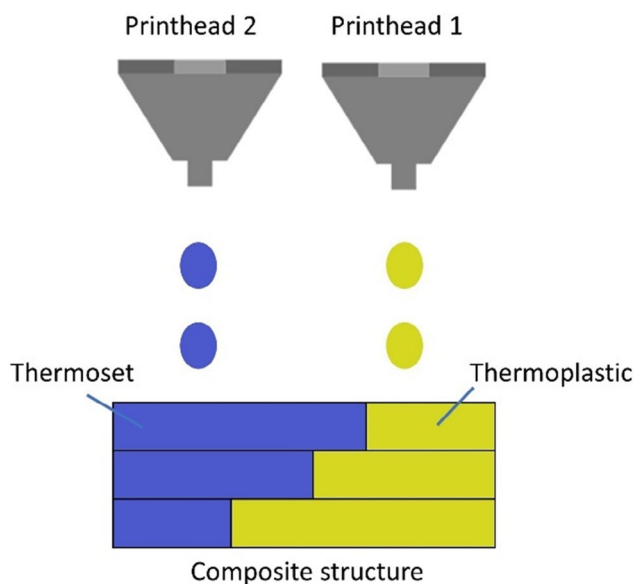


Figure 2. Diagram of two-color 3D printing.

powder particles, connecting them to form a 3D structure. For this work, a mixture of 1-hexanol and hexylacetate (Voxeljet, Augsburg, Germany) was used in the first printhead to generate the shape of the filler material. In the second printing head, a catalyst (tin–octoate, Sigma Aldrich, Hannover, Germany) was mixed to the same ink to induce the crosslinking of the MK polymer in the selected thermoset frame areas.

The printed part was then immersed in a water solution to partially compensate the gravitational force by buoyancy and annealed at a rate of $1.5\text{ }^{\circ}\text{C h}^{-1}$ to $55\text{ }^{\circ}\text{C}$, with a holding time of 2 h, followed by free cooling to room temperature. During this post treatment, the printed filler volume (without catalyst) melted and flowed under the driving force of surface tension, self-organizing into physical minimal surface area shapes while adapting to the boundary geometry, which is given by the stable printed frame (with catalyst). To balance the effects of gravity, the density of the water solution was matched to the density of the MK polymer. 10.5 wt% of copper sulfate was added to a saturated sodium chloride solution to increase the density to 1.25 g cm^{-3} , which is close to the density of the polymer. To remove air bubbles, the porous printed parts were immersed in water solution and placed in a vacuum oven at 25 mbar for a holding time of 15 min before the annealing treatments, to allow the water solution to fully infiltrate into open pores of the powdery printed preform. After slowly bringing back the setup to normal pressure, it was transferred to the annealing oven.

The obtained samples were scanned by μ computed tomography (CT) (μ CT 40, SCANCO MEDICAL AG, Switzerland) to analyze the microstructure. The scanned data was reconstructed with the VGStudio Max 2.2 (Volume Graphics GmbH, Heidelberg, Germany) software and compared to the original computer aid design (CAD) model to analyze the topological differences.

To characterize the surface quality of a self-organized part, a honeycomb flat structure was manufactured by the self-

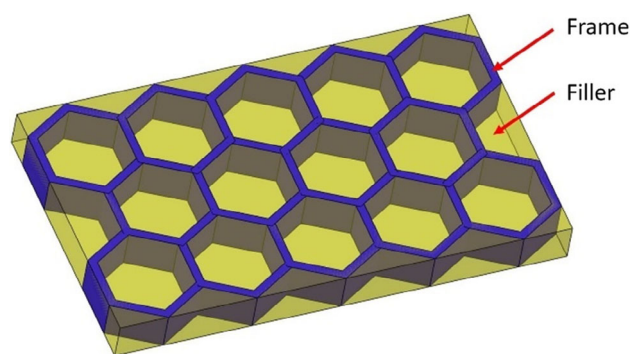


Figure 3. Frame–filler composite structure of honeycomb for free surface flow and self-organization.

organization process, following the same procedure used for the gyroid. **Figure 3** shows a model of the honeycomb, in which the frame in blue color was printed with catalyst, and the filler in yellow color was printed without catalyst.

The surface roughness of the honeycomb sample was quantified and analyzed by white light interference (3D Optical Surface Profiler, Nexview, Zygo Corporation, USA).

The particle alignment experiment was carried out with the same honeycomb geometry but adding 2.3 wt% of ferromagnetic MnZn–ferrite powders (Tridelta Weichferrite GmbH, Germany) to the MK powder (named as MK mixture) before printing and mixed homogeneously by TURBULA shaker mixer (Willy A. Bachofen AG, Switzerland) for 1 h at a speed of 45 cycles per minute. The particle size distribution of the ferromagnetic powder was $D_{10} = 2\text{ }\mu\text{m}$, $D_{50} = 8\text{ }\mu\text{m}$, and $D_{99} = 30\text{ }\mu\text{m}$ and the Curie temperature was $220\text{ }^{\circ}\text{C}$. This particle size as well as the low concentration ensured the homogeneous distribution in the MK powder ($D_{50} = 67\text{ }\mu\text{m}$), so that printing parameters were not affected, and the results were comparable to that from pure MK powder. One hexagon cell, as shown in **Figure 4**, was printed and the printed structure was then immersed in

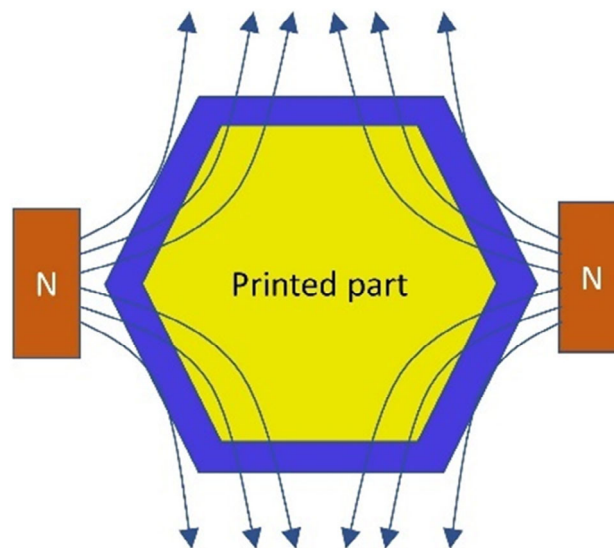


Figure 4. Illustration of self-organization under magnetic field.

saturated NaCl water solution and carefully annealed according to the self-organization process, as described earlier. During the self-organization process, a magnetic field was applied during thermal treatment. This was achieved by placing the printed part between two $25 \times 25 \times 13$ mm NdFeB-sintered ceramic magnets (Supermagnete, Germany), whose magnetic field strength at the surface was measured as 400 mT by a PCE-MFM 3000 Gaussmeter (PCE Instruments, Germany) in DC mode, as illustrated in Figure 4.

The magnetic field was manipulated by the distance and pole orientation. The alignment of the ferromagnetic particles was achieved in the configuration shown in Figure 4, with a distance of the N-to-N poles of 74 mm.

3. Results and Discussion

3.1. Gyroid Structure and Analysis

A gyroid is an infinitely connected TPMS. Therefore, it can be expected that this structure will survive local melting and surface tension driving viscous flow. The boundary conditions for the melting filler are given by the crosslinked frame surrounding the gyroid structure. The gravitational potential is nearly completely compensated by the water solution during the thermally induced self-organization. However, it should be mentioned that the densification of the polymer during self-organization induces an unbalance between buoyant force and gravitational force. The unbalanced force can drag the melted membrane away from a minimal surface, eventually causing a collapse. Therefore, the self-organization should not span over a large distance so that the membrane remains stable. The gyroid unit cell shown in Figure 1 approximately has the maximum size for which the structure is stable. There are two approaches possible to produce larger structures. The first possibility is to assemble multiple unit cells, each one with its own frame. For a 2D hexagonal unit cell, this corresponds to the example shown in Figure 3. Alternatively, a core–shell structure can be printed in which, for example, every strut of the geometry has a crosslinked core, and only the external shell can melt and self-organize. This latter strategy has been described in previous work by Zocca et al.^[18]

Figure 5 shows the gyroid-printed sample before and after self-organization. Figure 5a shows the structure after binder jetting,

which has rough surface and is highly porous, as can be recognized by its white appearance. Figure 5b shows the evolution of the same sample to an optical translucent structure after self-organization, following the geometry of a gyroid shape.

The reconstructed model from μ CT scanning is shown in Figure 5c. By cutting out the top surface of the 3D reconstruction, the filler after self-organization is visible, as schematically illustrated in the CAD model in Figure 1.

The comparison between the μ CT model of the printed gyroid and the corresponding CAD model is shown in Figure 6a.

The dimensional variation of the nonflowable frame compared to the CAD model is mostly in the range of ± 0.3 mm. This small deviation originates from the printing process and from deformations during annealing.

The filler remarkably differs from the CAD model by more than ± 1.0 mm. The difference is supposed to derive from the shape evolution of the film responding to the surrounding potentials, such as surface energy, gravity, and buoyancy. An additional influence is given by the partial infiltration of molten filler material into the porous frame, which is driven by capillary forces. This effect causes the membrane thickness to shrink from originally 3 mm to below 2 mm. As discussed in detail in a previous publication,^[14] the shape evolution during posttreatment is governed by an interplay between the viscous flow of the material infiltrating the frame (thus reducing the amount of molten filler available in the membrane) and the flow guided by surface tension, which leads to the minimization of surface energy for the given boundary conditions.

In Figure 6b, the green-colored line represents the theoretical membrane of a gyroid structure, while the gray-colored area represents the scanned bulk of the self-organized membrane. It shows that the self-organized material follows the shape of the theoretical membrane but a deviation. The surface energy is the main potential driving the shape evolution of the membrane into a minimal surface energy state.

It is important to point out that, although the part will eventually self-organize into a minimal surface energy state if given sufficient time, this will not correspond to that of a minimal surface gyroid in mathematical terms. An ideal minimal surface gyroid only exists when the thickness of membrane is zero, where the mean curvature as well as the curvature-induced pressure vanish. When the membrane has a certain thickness, the thickness brings additional pressure onto the surface of the

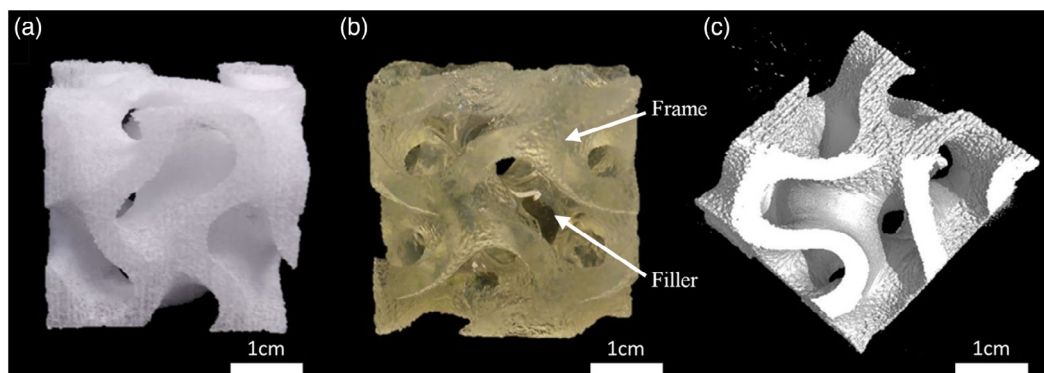


Figure 5. Photos of gyroid a) before, b) after self-organization, and c) internal section view from μ CT reconstruction.

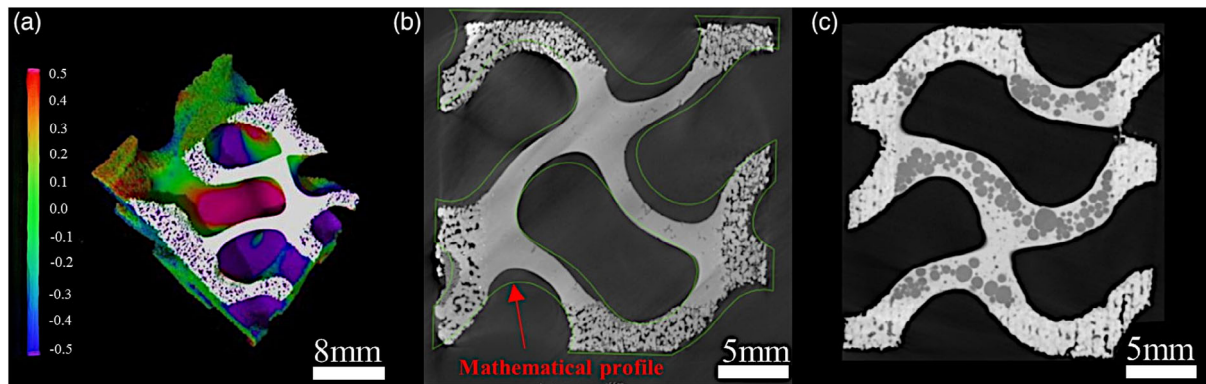


Figure 6. μ CT analysis of the self-organized gyroid structure. a) Deviation of the self-organized structure from the gyroid CAD model. b) Cross section of the 3D model in (a), showing the profile deviation of filler and frame from a theoretical gyroid profile. c) Gray value analysis in a cross section of the μ CT-reconstructed model. Many spherical bubbles were found with slightly higher density than the surrounding MK matrix. These bubbles appear to be water solution trapped in the polymer bulk.

membrane, which is termed Laplace pressure, causing deviation of the curvature from the mathematical minimal surface.

The pressure difference across a curved interface is described by the Young-Laplace equation as follows.

$$\Delta p = \gamma \left(\frac{1}{R_1} + \frac{1}{R_2} \right) \quad (2)$$

where Δp is the Laplace pressure across the interface in normal direction. γ is surface tension in the liquid at the liquid–gas interface. R_1 and R_2 are the principal radii of the curvature.

The equation indicates that the curvature of a surface causes a Laplace stress, which vanishes when the constant mean curvature of R_1 and R_2 is zero. At this point, the surface is named as minimal surface in mathematical terms.

In a gyroid with certain thickness such as in the experiment, the membrane has two surfaces and the stress on each surface does not merely come from the curvature, but it is in equilibrium also with the internal pressure and with additional force arising from the bulk of the material (e.g., gravitation). For this reason, a zero-mean curve as defined mathematically above cannot exist.

Additional variation is the shape and thickness of the membrane, which was found to vary between 1.27 and 1.88 mm, and can be induced by gravity, by the effect of the infiltration and by the slight deformations of the frame itself.

Figure 6c also shows a significant improvement of density in the self-organized material compared with the external frame. By analysis of the μ CT scan in VG Studio, the porosity was found to be reduced from 15.10 to 0.004 vol% by self-organization.

3.2. Optical Transparent Lens, Dimension, Transparency, and Surface Roughness

Figure 7a,b compares the honeycomb structure before and after self-organization. It shows the part evolution from opaque to optically transparent by the self-organization process, which indicates that the structure became fully dense and that surface roughness was significantly reduced. The surface of the filler area was characterized by white light interference, and representative images of the surface morphology before and after self-

organization are presented in Figure 8a,b respectively. Figure 7c,d shows a multilens array and a larger lens, demonstrating the potential of the self-organization process in producing optical application components. The biconcave curvature of the lens in Figure 7d is stabilized by surface tension, which tends to minimize the surface area, and it can be manipulated via tailoring the dimension of the frame and the mass amount of filler.

Figure 8 shows the scanning result of surface morphology. The height information of the morphology is highlighted by colors. The peaks and valleys on the rough surface before self-organization are clearly visible in Figure 8a, while the surface after self-organization is obviously flattened in Figure 8b. The surface roughness of the body as printed was estimated as $R_a = 60.3 \mu\text{m}$ within 1.6 mm linear measuring length in X and Y directions, while that after self-organization was in the range of 0.055–0.073 μm . After self-organization, as shown in Figure 8b, the surface not only became smoother, but also became concave, due to the material infiltrating the frame and self-organizing following the boundary conditions given by the frame. To avoid the influence of the curvature on the calculation of surface roughness, the scanning data from Nexview was flattened in the TrueSurf software (TrueGage Surface Metrology, USA) beforehand.

In the following sections, these results are compared to other typical AM technologies in terms of surface roughness. There are several literatures published that comprehensively review the surface quality among different AM processes.^[19,20] Figure 9 plots the surface roughness character according to AM processes and compares the self-organization effect in the general landscape.

Typically, material jetting can reach surface roughness R_a values in the range 5–10 μm , depending on the material characteristics and parameters used. Vat photopolymerization follows in a wider range of 10–50 μm . Powder-based and material extrusion technologies are known to produce higher surface roughness R_a , ranging from 20 to 60 μm for laser beam melting and to 40–120 μm for binder jetting and fused deposition modeling.

In particular, it is commonly accepted that binder jetting (powder bed 3D printing) generates parts with a rough

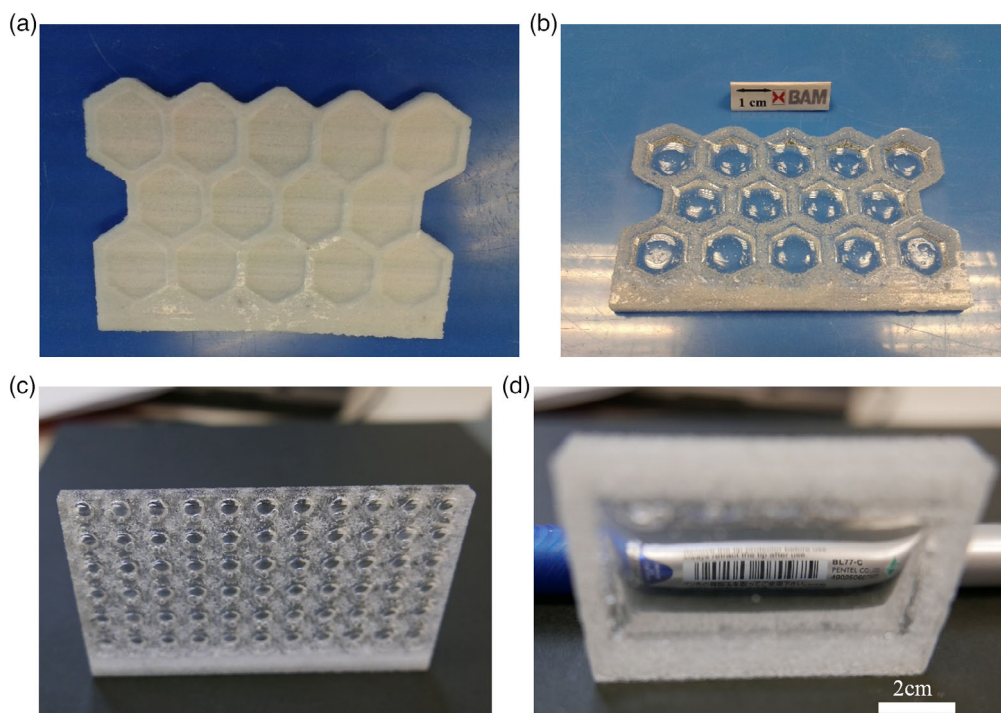


Figure 7. Honeycomb structure a) before and b) after self-organization and (c,d) optical transparent components produced by the same procedure.

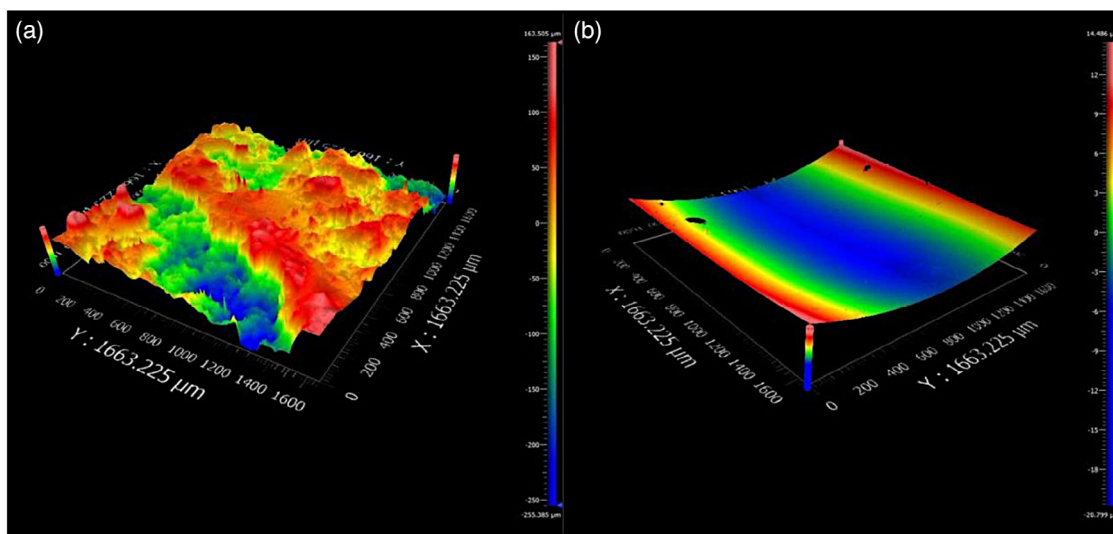


Figure 8. Surface reconstruction of parts before (left) and after (after) self-organization.

surface, which can often exceed R_a 100 μm. It is particularly noticeable that the self-organization of binder-jetted polymeric parts leads to surface roughness in the range of tenths of nanometers, which is a remarkable improvement by three orders of magnitude.

The result after self-organization is in fact comparable to the two-photon polymerization process, which currently can achieve the highest resolution in AM processes but only for very small parts and with low productivity. Applying the self-organization process to powder bed, 3DP is advantageous for both its high

production throughput and large dimension scale. Although there are specific restrictions for the materials and geometries that can be implemented, self-organization can open new design possibilities for the AM of optical lens, along with some other AM technologies.^[21]

3.3. Particle Alignment in Multipotential Field

Figure 10 shows the honeycomb structure before and after self-organization in a magnetic field. Figure 10a shows the as-printed

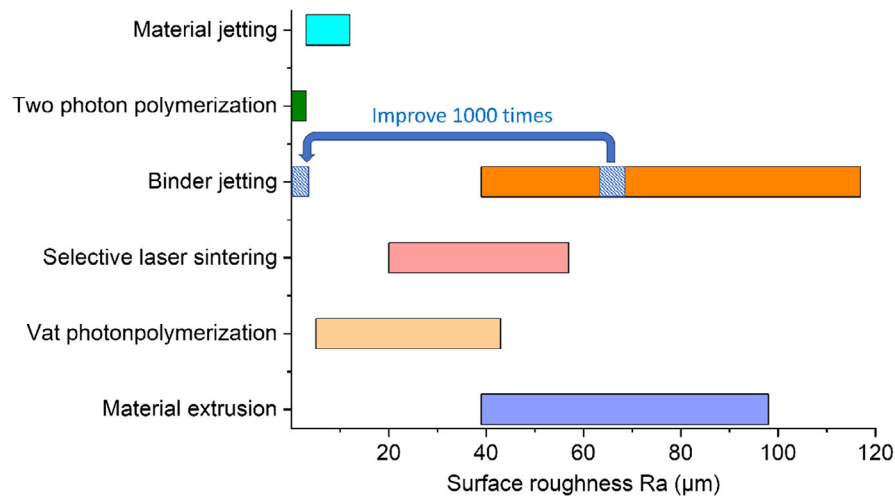


Figure 9. Comparison of surface roughness among AM techniques and self-organization.^[23–25]

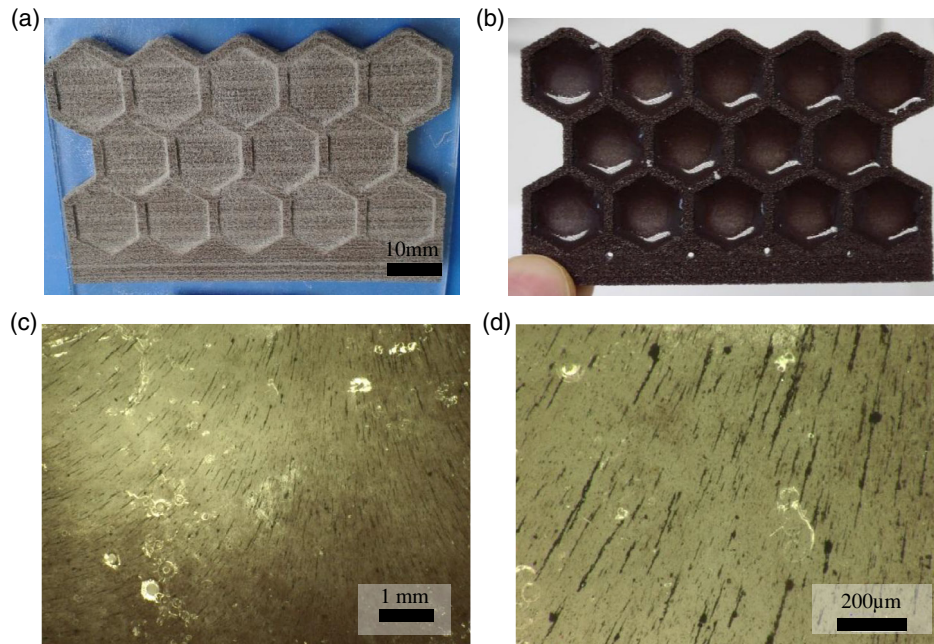


Figure 10. Particle alignment by multipotential self-organization.

honeycomb body from the MK mixture. It shows a strong brownish color because of the addition of ferromagnetic MnZn–ferrite powder. Figure 10b shows the same part after self-organization. Images of the filler area after particle alignment observed by optical microscopy are shown in Figure 10c,d. The particles align along the magnetic field lines to minimize their potential energy.

This experiment takes advantage of the possibility of manipulating the material while it is in a viscous state. On the one hand, this effect can be deleterious, such as that mentioned for the effect of an unbalanced gravitational field, leading to distortion of the object. On the other hand, external potentials can be applied on purpose to modify the shape or

the microstructure of the material, as shown here provided by a magnetic field.

4. Conclusion

The local melting self-organization process is demonstrated to have the potential to significantly decrease the surface roughness of 3D-printed parts, while structural elements of minimal surface are obtained.

Upgrading the self-organization concept from a 2D to 3D geometry allows taking inspiration from minimal surface geometries for lightweight structure design, which follows the

principle of achieving maximum load capacity using minimal amount of material and even distribution of stresses. As soap films are commonly used as analog physical models for mathematical minimal surfaces, 3D-printed and self-organized structures can also be used as models for bulk structures in which the boundary geometry can be flexibly defined.

An exemplary honeycomb part showed an improvement from surface roughness $R_a \approx 60 \mu\text{m}$ after printing to $R_a \approx 0.05\text{--}0.07 \mu\text{m}$ after self-organization, which is a three orders of magnitude difference. At the same time, the printed opaque structure was transformed into an elegant array of optically transparent lenses, showing that the homogeneity of the material is also improved, due to a reduction in porosity.

In the further developed concept of the as-presented surface energy-driven self-organization, the 3D-printed part can be manipulated by deliberately introducing additional potential energy fields, such as gravity and electromagnetic fields. This approach was demonstrated by placing a 3D-printed part in a magnetic field to align ferromagnetic MnZn–ferrite powder in the polymeric transient molten phase during self-organization, thus tailoring the microstructural texture of the material. This method is not limited to magnetic potentials to manipulate ferrite powder, but it is also applicable to other potentials to control discrete phases in the matrix providing specific functions. The same concept can be followed by adding, for example, carbon nanotubes,^[22] SiC particles, to achieve tunable properties and could be applied in fabricating sensors for thermal, optical, and mechanical testing. Further research in the particle alignment is expected to be carried out in the future.

Acknowledgements

Open access funding enabled and organized by Projekt DEAL.

Conflict of Interest

The authors declare no conflict of interest.

Data Availability Statement

The data that support the findings of this study are available on request from the corresponding author. The data are not publicly available due to privacy or ethical restrictions.

Keywords

additive manufacturing, functional structures, programmable materials, self-organizations

Received: September 16, 2021

Revised: November 16, 2021

Published online:

- [1] C. Flaviana, *Virtual and Physical Prototyping*, Taylor and Francis Ltd., London, UK **2018**, p. 13.
- [2] E. Maleki, S. Bagherifard, M. Bandini, M. Guagliano, *Additive Manuf.* **2021**, *37*, 101619.
- [3] R. Anitha, S. Arunachalam, P. Radhakrishnan, *J. Mater. Process. Technol.* **2001**, *118*, 385.
- [4] B. Vasudevarao, D. P. Natarajan, M. Henderson, in *Int. Solid Freeform Fabrication Symp.*, University of Texas, Austin, USA **2000**.
- [5] A. Antonio, *Rapid Prototyping J.* **2006**, *12*, 1.
- [6] P. B. Bacchewar, S. K. Singhal, P. M. Pandey, *Proc. Inst. Mech. Eng., Part B: J. Eng. Manuf.* **2007**, *221*, 35.
- [7] T. Nancharaiyah, D. Ranga Raju, V. Ramachandra Raju, *Int. J. Emerg. Technol.* **2010**, *1*, 106.
- [8] N. Turner Brian, S. A. Gold, *Rapid Prototyping J.* **2015**, *21*, 250.
- [9] S. K. Everton, M. Hirsch, P. Stravroulakis, R. K. Leach, A. T. Clarea, *Mater. Des.* **2016**, *95*, 431.
- [10] U. Ali, H. Fayazfar, F. Ahmed, E. Toyserkani, *Vacuum* **2020**, *177*, 109314.
- [11] N. N. Kumbhar, A. V. Mulay, *J. Inst. Eng. (India)* **2018**, *99*, 481.
- [12] C.-C. Kuo, C.-M. Chen, S.-X. Chang, *Int. J. Adv. Manuf. Technol.* **2017**, *91*, p3211.
- [13] H. Raggelle, M. W. Tibbitt, S.-Y. Wu, M. A. Castillo, G. Z. Cheng, S. P. Gangadharan, D. G. Anderson, M. J. Cima, R. Langer, *Nat. Commun.* **2018**, *9*, 1184.
- [14] J. Chi, A. Zocca, B. A. Blanco, J. Melcher, M. Sparenberg, J. Günster, *Adv. Mater. Technol.* **2018**, *3*, 1800003 1.
- [15] S. Dutta, S. Chattopadhyay, A. Sarkar, M. Chakrabarti, D. Sanyal, D. Jana, *Progr. Mater. Sci.* **2009**, *54*, 89.
- [16] G. L. Messing, S. Trolier-McKinstry, E. M. Sabolsky, C. Duran, S. Kwon, B. Brahmaraout, P. Park, H. Yilmaz, P. W. Rehrig, K. B. Eitel, E. Suvaci, M. Seabaugh, K. S. Oh, *Crit. Rev. Solid State Mater. Sci.* **2004**, *29*, 45.
- [17] A. Kotikian, R. L. Truby, J. W. Boley, T. J. White, J. A. Lewis, *Adv. Mater.* **2018**, *30*, 1706164.
- [18] A. Zocca, C. Gomes, U. Linow, H. Marx, J. Melcher, P. Colombo, J. Günster, *Rapid Prototyping J.* **2016**, *22*, p344.
- [19] J.-Y. Lee, J. An, C. K. Chua, *Appl. Mater. Today* **2017**, *7*, 120.
- [20] A. M. Syed, T. Elias, P. Koumoulos, A. Bandyopadhyay, S. Bose, L. O'Donoghue, C. Carotids, *Materials Today* **2018**, *21*, 22.
- [21] A. Zolfaghari, T. Chen, A. Y. Yi, *Int. J. Extreme Manuf.* **2019**, *1*, 012005.
- [22] X. Zhang, C. L. Pint, M. H. Lee, B. E. Schubert, A. Jamshidi, K. Takei, H. Ko, A. Gillies, R. Bardhan, J. J. Urban, M. Wu, R. Fearing, A. Javey, *Nano Lett.* **2011**, *11*.
- [23] W. E. Frazier, *J. Mater. Eng. Perform.* **2014**, *23*, 1917.
- [24] A. Townsend, N. Senin, B. Liam, R. K. Leach, J. S. Taylor, *Prec. Eng.* **2016**, *46*, 34.
- [25] S. C. Ligon, R. Liska, J. Stampfl, M. Gurr, R. Mülhaupt, *Chem. Rev.* **2017**, *117*, p3239.